

Time varying polarized gamma-rays from GRB 160821A: evidence for ordered magnetic fields

VIDUSHI SHARMA,¹ SHABNAM IYYANI,¹ DIPANKAR BHATTACHARYA,¹ TANMOY CHATTOPADHYAY,^{2,3} A. R. RAO,^{1,4}
E. AARTHY,⁵ SANTOSH V. VADAWALE,⁵ N. P. S. MITHUN,⁵ VARUN. B. BHALERAO,⁶ FELIX RYDE,^{7,8} AND
ASAF PE'ER^{9,10}

¹*Inter-University Center for Astronomy and Astrophysics, Pune, Maharashtra 411007, India*

²*Department of Physics, Stanford University, 382 Via Pueblo Mall, Stanford CA 94305*

³*Kavli Institute of Astrophysics and Cosmology, 452 Lomita Mall, Stanford, CA 94305*

⁴*Tata Institute of Fundamental Research, Mumbai, Maharashtra 400005, India*

⁵*Physical Research Laboratory, Ahmedabad, Gujarat 380009, India*

⁶*Indian Institute of Technology Bombay, Mumbai, India*

⁷*Department of Physics, KTH Royal Institute of Technology, AlbaNova, SE-106 91 Stockholm, Sweden*

⁸*The Oskar Klein Centre for Cosmoparticle Physics, AlbaNova, SE-106 91 Stockholm, Sweden*

⁹*Department of Physics, University College Cork, Cork, Ireland*

¹⁰*Department of Physics, Bar-Ilan University, Ramat-Gan, 52900, Israel*

(Received July , 2019; Revised xxx, 2019; Accepted xxx,xxx)

Submitted to ApJL

ABSTRACT

GRB 160821A is the third most energetic gamma ray burst observed by the *Fermi* gamma-ray space telescope. Based on the observations made by Cadmium Zinc Telluride Imager (CZTI) on board *AstroSat*, here we report the most conclusive evidence to date of (i) high linear polarization ($66^{+26}_{-27}\%$; 5.3σ detection), and (ii) variation of its polarization angle with time happening twice during the rise and decay phase of the burst at 3.5σ and 3.1σ detections respectively. All confidence levels are reported for two parameters of interest. These observations strongly suggest synchrotron radiation produced in magnetic field lines which are highly ordered on angular scales of $1/\Gamma$, where Γ is the Lorentz factor of the outflow.

Keywords: gamma-ray burst - polarization - radiation mechanisms: synchrotron

1. INTRODUCTION

Gamma-ray bursts (GRBs) are the most intense astrophysical outbursts in the Universe. In the last several decades, the spectra of prompt gamma-ray emission of GRBs have been extensively studied using various space observatories like BATSE onboard CGRO (Fishman 2013), *Niel Gehrels Swift* (Gehrels & Swift 2004), *Fermi* (Meegan et al. 2009; Atwood et al. 2009) etc. The radiation process producing the prompt gamma-ray emission, however, still remains a mystery. Polarization along with spectrum measurements can provide an insight into this long standing enigma. Polarization measurement of prompt emission is highly challenging, mainly because of the scarcity of incident photons and the brevity of the event. Previously, polarization measurements of prompt gamma ray emission were attempted only for a few cases by RHESSI (Coburn & Boggs 2003; Wigger et al. 2004), INTEGRAL (McGlynn et al. 2009; Götz et al. 2009, 2013, 2014), GAP (Yonetoku et al. 2011, 2012), CZTI (Rao et al. 2016; Chattopadhyay et al. 2017; Chand et al. 2018, 2019), POLAR (Zhang et al. 2019; Burgess et al. 2019) etc but the results were statistically less significant and sometimes unconvincing (for a recent review please refer McConnell 2017). In this Letter, for the first time, we present a conclusive evidence of polarization across the GRB 160821A in the energy range 100 – 300 keV using CZTI (Cadmium Zinc Telluride Imager) instrument aboard *AstroSat* (Singh et al. 2014).

On August 21, 2016 the Burst alert telescope (BAT) on board *Neil Gehrels Swift* observatory (Gehrels & Swift 2004), triggered and located the GRB 160821A at (RA, Dec) = (171.248, 42.343) with 3 arcmin uncertainty (Markwardt et al. 2016) at 20:34:30 UT, along with other space observatories such as Konus-wind and the Gamma-Ray Burst monitor on board CALET. However, due to solar observing constraints *Swift* could not slew to the BAT position until a week. Hence, there was no X-ray Telescope (XRT) and UV/Optical Telescope (UVOT) observations for this burst. Half an hour after the trigger time, an optical transient was detected by ground based telescopes but no redshift measurement could be made.

Fermi Gamma-Ray Burst Monitor (GBM, Meegan et al. 2009) also triggered on the burst at 20:34:30.04 UT (Stanbro & Meegan 2016). The GBM light curve included a precursor emission starting from trigger time, T_0 till $T_0 + 112$ s, followed by a bright emission episode with a duration T90¹ of 43 s. For the time interval $T_0 - 4.1$ s to $T_0 + 194.6$ s, an energy flux of $2.86 \pm 0.007 \times 10^{-6}$ erg/cm²/s is obtained in 10-1000 keV band. This makes the burst the third brightest GRB observed by *Fermi* till date in terms of energy flux. The *Fermi*-Large Area telescope (LAT, Atwood et al. 2009) detected emission in the LAT Low Energy (LLE) data (30 – 100 MeV), starting at $T_0 + 116$ s and emission above 100 MeV starting at $T_0 + 130$ s (Arimoto et al. 2016), with LAT emission extending up to ~ 2000 s beyond the duration of GBM emission. *AstroSat*-CZTI also detected the burst for a duration T90 of 42 s (Bhalerao et al. 2016) and captured only the main episode of the burst. GRB 160821A was incident on CZTI from the direction, $\theta = 156.2^\circ$ and $\phi = 59.2^\circ$, thus coming through the side veto detector. Polarization measurement was attempted in the energy range 100 - 300 keV using ~ 2549 detected Compton events (Chattopadhyay et al. 2014, 2017). In Figure 1a, a composite 1 s binned light curve obtained from various detectors on board *Fermi*, *AstroSat* and *Swift* satellites are shown. The present work focuses only on the results of the study of the main episode of the burst observed by both *Fermi* and *AstroSat*.

2. POLARIZATION ANALYSIS

The measurement of polarization is obtained from the azimuthal distribution of Compton scattered photons, which lie preferentially in a direction orthogonal to the incident electric field vector (Covino & Gotz 2016; McConnell 2017). The azimuthal distribution is fitted with the cosine function of the form,

$$C(\eta) = A \cos(2(\eta - \phi_0 + \pi/2)) + B \quad (1)$$

where ϕ_0 is the polarization angle (PA) of the incident photons as measured in the CZTI detector plane, A/B is the modulation factor (μ) and η is the azimuthal angle (also see Zhang et al. 2019). The measured detector plane PA is converted into the celestial/ sky reference frame by taking into account the satellite orientation at the time of observation and these values are reported throughout the Letter unless otherwise mentioned. The polarization fraction (PF) is calculated by normalizing the modulation with μ_{100} (the modulation factor obtained for 100% polarized emission coming from the same direction of the GRB with the same spectrum) for the respective detector PA.

A low polarization (PF = 21_{-19}^{+24} %) was found at 90% (2.2σ) confidence level for two parameters of interest, when the entire pulse constituting a time interval of 115 - 155 s was analyzed (Figure 1b). All the errors quoted for polarization measurements in the Letter are at 68% confidence interval of two parameters of interest including the systematic errors (Appendix A) unless otherwise mentioned. We find this result to be in agreement with the recent polarization observations of GRBs made by POLAR (Zhang et al. 2019), where they find the time integrated emission of GRBs to possess a low polarization fraction. They suspect that such low polarization could be due to change in polarization angle within the pulses/ across different pulses.

The evolution of the light curves observed by *Fermi* in different energy bands were characterized by studying the ratio of photon counts observed in high and low energies, parameterized as the hardness ratio (HR), see panels 1 and 2 in Figure 1c. We found that the emission above 30 MeV changed distinctly with respect to the rest of the burst after $T_0 + 129$ s and $T_0 + 140$ s. In addition to this, a fine time resolved polarization analysis of the main episode was conducted. Polarization fraction and polarization angle for successive 10 s intervals shifted by 2.5 s were measured, thereby studying the evolutionary trend in PF and PA (Figure 1c). Such a methodology including overlapping time intervals was adopted because of the limited number of photons available in the smaller time intervals. Therefore, during the analysis we tried to constrain the PF such that at least the lower limit of 68% confidence interval of one parameter of interest was greater than zero. This is because if the time interval is unpolarized i.e PF is consistent

¹ T90 for *Fermi* (or *AstroSat*) is defined as the time duration between the epochs when 5% and 95% of the total photon counts of the burst are detected in the energy range 50 -300 keV (40-200 keV).

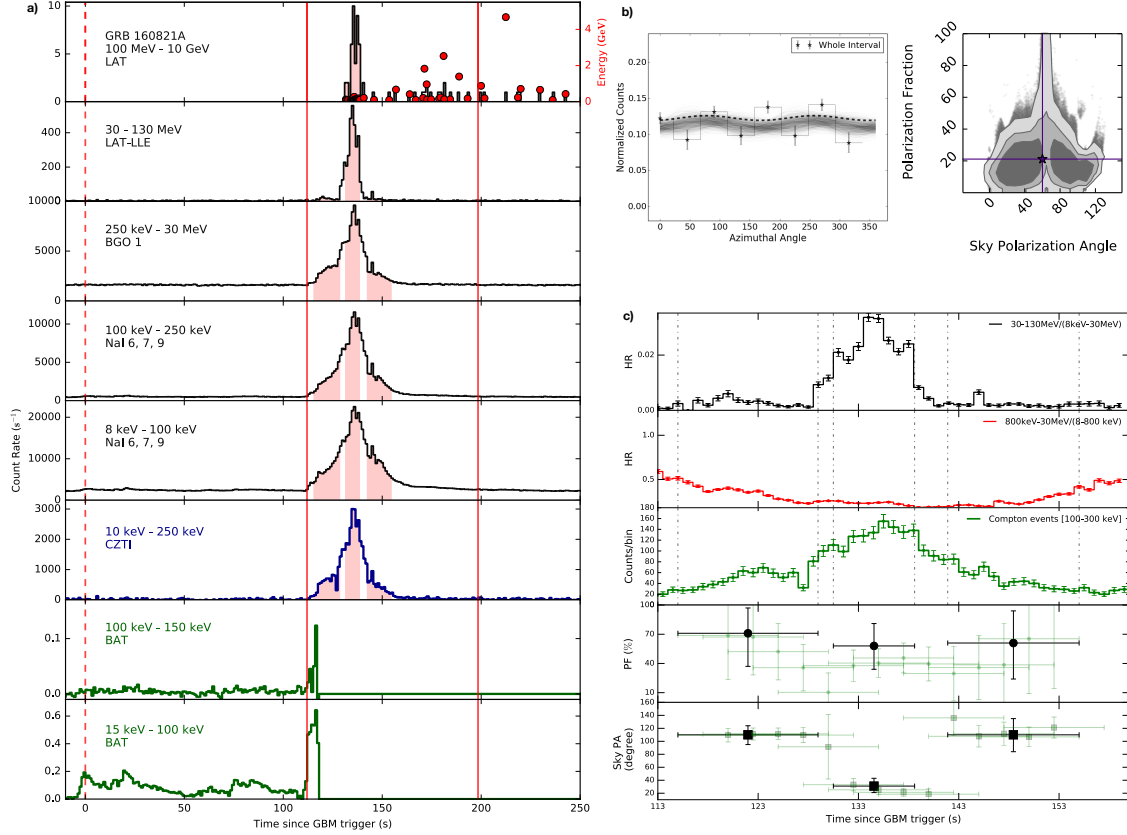


Figure 1. a) A composite 1 s binned light curve of the burst is shown for *Fermi* detectors: LAT, LAT-LLE, BGO and NaI, *AstroSat*/ CZTI and *Swift*/ BAT. The red vertical dashed line (at $T_0 = 0$ s) corresponds to the trigger time of *Fermi* and the red solid vertical lines mark the beginning and end of the main episode of the burst. The *Fermi*/LAT photons whose probability of association with the same GRB is greater than 90%, are shown as red points in the upper panel with energy information scaling on the right side of y-axis. The time intervals studied in polarization analysis are shown in shaded red regions. b) On the left, the azimuthal distribution and the best fit modulation (dashed line) obtained for the entire main episode of the burst are shown. Modulation fits obtained for 1000 runs out of the 1.1×10^7 simulation datasets are shown in the shaded black colour. On the right, the 2D histogram plot of the obtained PF and PA values along with the contours corresponding to confidence levels of 68%, 90%, 99% are shown in darker to lighter colors of black which are over plotted on the scatter plot of PF and PA. The average value of PF and PA are marked by the violet star. c) Uppermost and second top panels show the hardness ratio (HR) of the counts LLE to sum of the counts in NaI 6 and BGO 1 (black), and ratio of the counts in BGO 1 to that of NaI 6 respectively. In the third panel, the 1s binned CZTI Compton events (green) light curve is shown. The time intervals (black vertical dash dot lines) for which the temporal polarization study is done, are shown. Fourth and fifth panels show the polarization fraction (PF, black circles) and corresponding polarization angle (PA, black squares) obtained for these time intervals. Also, PF and PA values obtained in the fine time resolved analysis are shown in the background in shaded green circles and squares respectively.

with zero, then its PA has no physical meaning. A change in PA was observed to occur twice as the burst transitioned from its rise to peak and later to its decay phases while PF was greater than zero.

We note that during the times when the PA angle makes a change, a decrease in PF is expected. Thus, based on the clear change in PA where we could constrain the polarization at a higher significance (i.e. the lower limit of 99% confidence interval of two parameters of interest of PF lie greater than zero) and the observed change in HR at high energies, we performed a relatively coarser time-resolved polarization analysis of the GRB by dividing the main episode into three non-overlapping time intervals: 115-129 s, 131-139 s and 142-155 s, which correspond to the rise, peak and decay phase of the burst respectively.

2.1. Results

During the first time interval, the burst emission has a polarization fraction of 71^{+29}_{-41} % and a polarization angle of 110^{+14}_{-15} °. In the second interval, a $PF = 58^{+29}_{-30}$ % with a corresponding $PA = 31^{+12}_{-10}$ ° and in the third interval, a $PF = 58^{+29}_{-30}$ % with a corresponding $PA = 31^{+12}_{-10}$ °.

$= 61_{-46}^{+39}\%$ with a corresponding $PA = 110_{-26}^{+25}^\circ$, are determined (Figure 1c). By performing Monte Carlo simulations (Appendix B) of the dataset of each interval, the posterior distributions of PF and PA of these intervals were also obtained. Intervals 1, 2 and 3 were found to be polarized at confidence levels of 99.8% (3.5σ), 99.97% (4σ) and 99.1% (3.1σ) respectively for two parameters of interest (Figure 2). As the burst transits from its rise to the peak phase and then into its decay phase, the PA shifts by $81^\circ \pm 13^\circ$ and $80^\circ \pm 19^\circ$ respectively (Figure 1c). The statistical significance of the change in polarization angles, ΔPA_1 and ΔPA_2 are determined at 3.5σ and 3.1σ respectively, which are the minimum of the obtained statistical significance of the two intervals to be polarized. Other cases of varying polarization that were reported earlier were GRB 041219A (Götz et al. 2009), GRB 100826A (Yonetoku et al. 2011) and GRB 170114A (Zhang et al. 2019) observed by *INTEGRAL*, GAP and POLAR respectively. The low PF, thus, found across the burst can now be understood as an artefact of the temporal change of PA occurring within the burst. The results of the polarization analysis of the three time intervals are listed in Table 1.

In order to estimate the average PF across the burst: (a) the first and the third intervals were combined since they had nearly same polarization angles (fourth panel of Figure 1 c); (b) Monte Carlo simulations involving combined fits of this new interval and the second interval with the cosine function were performed. The polarization fraction related parameters A and B of the cosine functions were linked across the intervals, while the polarization angles were kept free. Thus, we found the average polarization fraction and the polarization angles for the new interval and the second interval. In Figure 3, the posterior distributions of the average PF across the burst and the corresponding change in polarization angle estimated by taking the difference of the PAs of the new interval and interval 2 are shown. The average polarization fraction across the burst is estimated to be $66_{-27}^{+26}\%$ at 99.99992% (5.3σ) confidence for two parameters of interest as shown in Figure 3. Also, we note that the change in polarization angle estimate ($80_{-18}^{+17}^\circ$) is consistent with the average of the change in polarization angles that were found occurring within the burst. Previously, such a high statistically significant polarization was reported for the burst GRB 021206 by Coburn & Boggs (2003), however, the claim was contested by the analyses done by Rutledge & Fox (2004) and Wigger et al. (2004) subsequently. Recently, POLAR found that the time integrated emission of 5 bright GRBs observed by them, possess the most probable polarization fraction between 4% and 11% at a confidence level of 99.9% (Zhang et al. 2019). Till date no other polarization measurement of GRBs reported by BATSE, *INTEGRAL*, GAP, *AstroSat* and POLAR have obtained a statistical significance greater than $\sim 99.9\%$ (Zhang et al. 2019; Covino & Gotz 2016; McConnell 2017).

3. SPECTRAL ANALYSIS

Traditionally, the GRB prompt emission spectrum is modelled using the phenomenological Band function² (Band et al. 1993). The time resolved spectral analysis of the main episode of the burst, however, shows significant deviations from the pure Band function in the brightest bins (Preece et al. 2014; Vianello et al. 2018). The deviation in lower energies is modelled by adding a blackbody (BB) function at $kT \sim 30$ keV and that at higher energies by adding a cutoff at $E_c \sim 2 - 50$ MeV (Appendix C). Thus, the spectrum is best modelled using a blackbody + Band \times Hightcut (Figure 4a), where the blackbody can be related to the thermal emission, a relic of the dense fireball formed at the central engine after the explosion, and the rest to the non-thermal emission coming from the optically thin region of the outflow (Guiriec et al. 2011; Axelsson et al. 2012; Iyyani et al. 2013; Burgess et al. 2014; Iyyani et al. 2016; Vianello et al. 2018). The evolution of the spectral fit parameters are shown in Figure 4b. We note that the low energy part of the spectrum characterized by the low energy power law index, α and the spectral peak, E_p are nearly steady throughout at ~ -0.97 and 800 keV respectively. However, the high energy part of the spectrum characterized by the high energy power law index, β and cutoff, E_c vary significantly such that β decreases, whereas E_c increases with time and after $T_0 + 140$ s, these trends are reversed. This spectral behaviour is consistent with the trend observed in HR reported above.

4. DISCUSSION AND SUMMARY

GRBs with long durations, > 2 s, are associated with the death of massive stars. A highly collimated outflow (jet) of opening angle θ_j , moving at a relativistic speed (parameterized by Lorentz factor³, Γ) is produced after the core of the massive star collapses to a black hole (or a magnetar) and begins to accrete the surrounding stellar matter. The radiation emitted from this relativistic outflow is beamed towards the observer within a cone of $1/\Gamma$ which is thus, the visible region around the line of sight. This is referred to as the relativistic aberration/ beaming.

² Band function is an empirical function consisting of two power laws smoothly joined at a peak.

³ $\Gamma = 1/\sqrt{1 - (v/c)^2}$ where v is the velocity of the outflow and c is the speed of light.

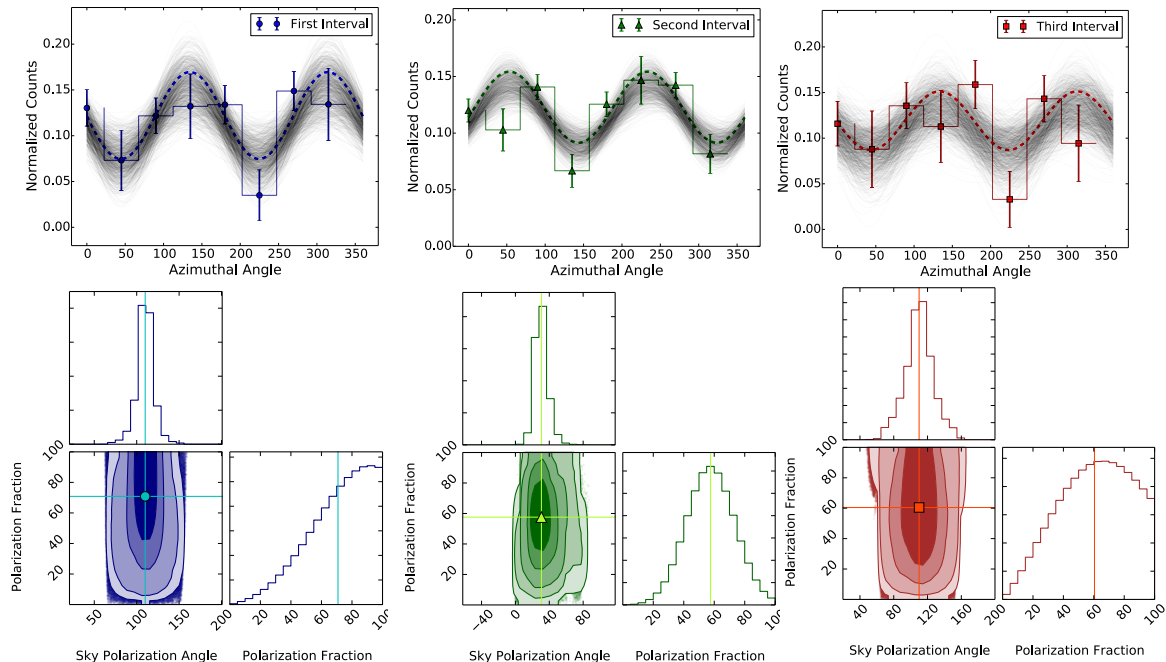


Figure 2. In the left top corner, for the first interval, the best fit modulation curve obtained is shown in blue dashed line. Modulation fits obtained for 1000 out of $\sim 10^7$ simulated data sets are shown here in shaded black color. In the left bottom corner the 2D histogram plot of the obtained PF and PA values, along with the contours corresponding to confidence levels of 68%, 90%, 99% and 99.9% are shown in terms of darker to lighter color shades of blue which are over-plotted on the scatter plot of PF and PA. Similar corresponding plots for the interval 2 are shown in the top middle and bottom middle (green colour). For this time interval, an additional contour of confidence level 99.99% is shown in the 2D histogram plot. For interval 3, corresponding plots are shown in the right top corner and right bottom corner (red colour). The average values of PF and PA obtained in the intervals 1,2,3 are marked by the blue circle, green triangle and red square respectively on their 2D histograms and they are marked by solid lines on their respective posterior distribution plots as well.

In a classical fireball model (Mészáros 2006; Pe’er 2015; Iyyani 2018), where the outflow is non-magnetized, the non-thermal emission is generally expected to be produced in shocks created in the optically thin region above the photosphere from where the thermal emission is expected. Energetic electrons produced in the shocks then cool by processes like synchrotron emission in random magnetic fields generated in the shocks (Ghisellini & Lazzati 1999), or inverse Compton scattering (Lazzati et al. 2004), both being inherently locally axisymmetric around the outflow’s velocity vector. For a fixed viewing angle⁴, $\theta_v > 0$, in an axially symmetric jet, the polarization vector integrated over the spatially unresolved emitting region, should point either perpendicular to or in the plane containing the axis of the jet and the line of sight of the observer. Thus, the PA is expected to change by 90° when the width of the jet parameterized by $\Gamma \theta_j$ changes. In such a case, when the orientation of the polarization vector becomes perpendicular to the observer plane, the polarization fraction is expected to be low, $< 10\%$ (Toma et al. 2009; Granot 2003; Ghisellini & Lazzati 1999). However, here we observe that during the entire burst, the PF values are $> 15\%$. Thus, a change in width of the visible portion of the jet cannot account for the observed change in PA. Inherently axisymmetric emission models referred to above are ruled out.

The total radiative energy⁵ released in the prompt emission of GRB 160821A is estimated to be $E_{\gamma, \text{iso}} = 6.9 \times 10^{53}$ (3.6×10^{55}) erg, for a redshift, $z = 0.4$ (2), if the radiation were isotropic. These are among the highest known values for long GRBs (Racusin et al. 2011). Such a high $E_{\gamma, \text{iso}}$ suggests that the emission is strongly collimated, with the jet pointing towards the observer such that the line of sight lies within the jet cone or just outside the edge of the jet ($\theta_j + 1/\Gamma$). In the above scenario, the strong observed polarization can be explained only by synchrotron emission produced in magnetic fields that are highly ordered within the viewing cone of $1/\Gamma$.

⁴ θ_v is the angle between the line of sight of the observer and the jet axis.

⁵ We find a fluence of $1.3 \pm 0.03 \times 10^{-3}$ erg/cm² in 10 keV - 5 GeV. Fluence is the energy flux integrated over the duration of the burst. We assume a flat Universe ($\Omega_\lambda = 0.73$ and $H_0 = 71$ km s⁻¹ Mpc⁻¹).

Table1. Results of the temporal polarization analysis.* The average values of μ , PF and PA from the posterior distribution are reported.

Time Intervals (s)	115-129	131-139	142-155
Compton events	896	1124	523
Background events (s^{-1})	20.7 ± 4.5	20.7 ± 4.5	20.7 ± 4.5
MDP (99% confidence)	40%	32%	57%
μ^*	0.289	0.250	0.243
μ_{100}	0.409	0.435	0.403
PF*	71^{+29}_{-41} %	58^{+29}_{-30} %	61^{+39}_{-46} %
PA*	110^{+14}_{-15} °	31^{+12}_{-10} °	110^{+25}_{-26} °
Confidence level	99.8%	99.97%	99.1%

If we assume the observed burst emission is a single emission episode, the observed high polarization along with a change in polarization angle is challenging to be explained in any known physical model. On the other hand, it can also be envisaged that the burst emission consists of multiple emission episodes and depending on the dominance of the synchrotron emissions coming from the different regions, a change in polarization angle can happen with time (also see [Lazzati & Begelman 2009](#)).

Thus, for the first time a conclusive evidence of high and varying linear polarization is detected in a GRB. The observations are extremely constraining and challenging for currently proposed physical models for gamma-ray bursts. This motivates further research into the development of a physical scenario that can explain the observations self consistently.

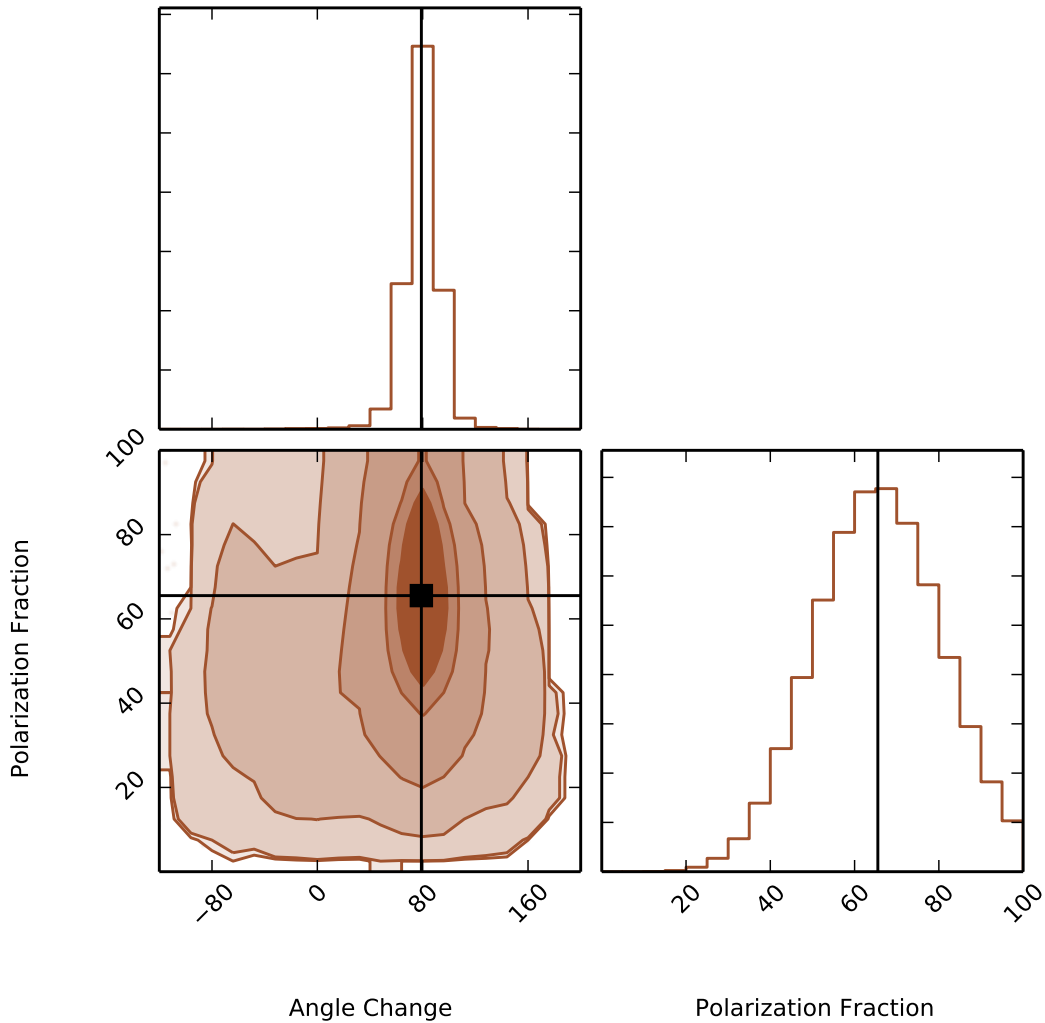


Figure 3. Above a 2D histogram plot of the average PF and correspondingly obtained average change in polarization angle, across the burst is shown. Contours corresponding to confidence levels 68%, 90%, 99.7%, 99.99%, 99.99992% (5.3σ) and 99.99995% (5.4σ) are shown. The average values of PF and change in PA are marked on their respective posterior distributions by a black solid line.

REFERENCES

- Arimoto, M., Axelsson, M., Dirirsa, F., & Longo, F. 2016, GRB Coordinates Network, Circular Service, No. 19836, #1 (2016), 19836
- Arnaud, K. A. 1996, in *Astronomical Society of the Pacific Conference Series*, Vol. 101, *Astronomical Data Analysis Software and Systems V*, ed. G. H. Jacoby & J. Barnes, 17
- Arnaud, K. A. 2013, in *AAS/High Energy Astrophysics Division*, Vol. 13, *AAS/High Energy Astrophysics Division #13*, 117.04
- Atwood, W. B., Abdo, A. A., & et al. 2009, *ApJ*, 697, 1071
- Axelsson, M., Baldini, L., & et al. 2012, *ApJ*, 757, L31
- Band, D., Matteson, J., & et al. 1993, *ApJ*, 413, 281
- Bhalerao, V., Kumar, V., Bhattacharya, D., Rao, A. R., & Vadawale, S. 2016, GRB Coordinates Network, Circular Service, No. 19867, #1 (2016), 19867
- Burgess, J. M., Kole, M., Berlato, F., et al. 2019, *A&A*, 627, A105
- Burgess, J. M., Preece, R. D., & et al. 2014, *ApJ*, 784, 17
- Cash, W. 1979, *ApJ*, 228, 939

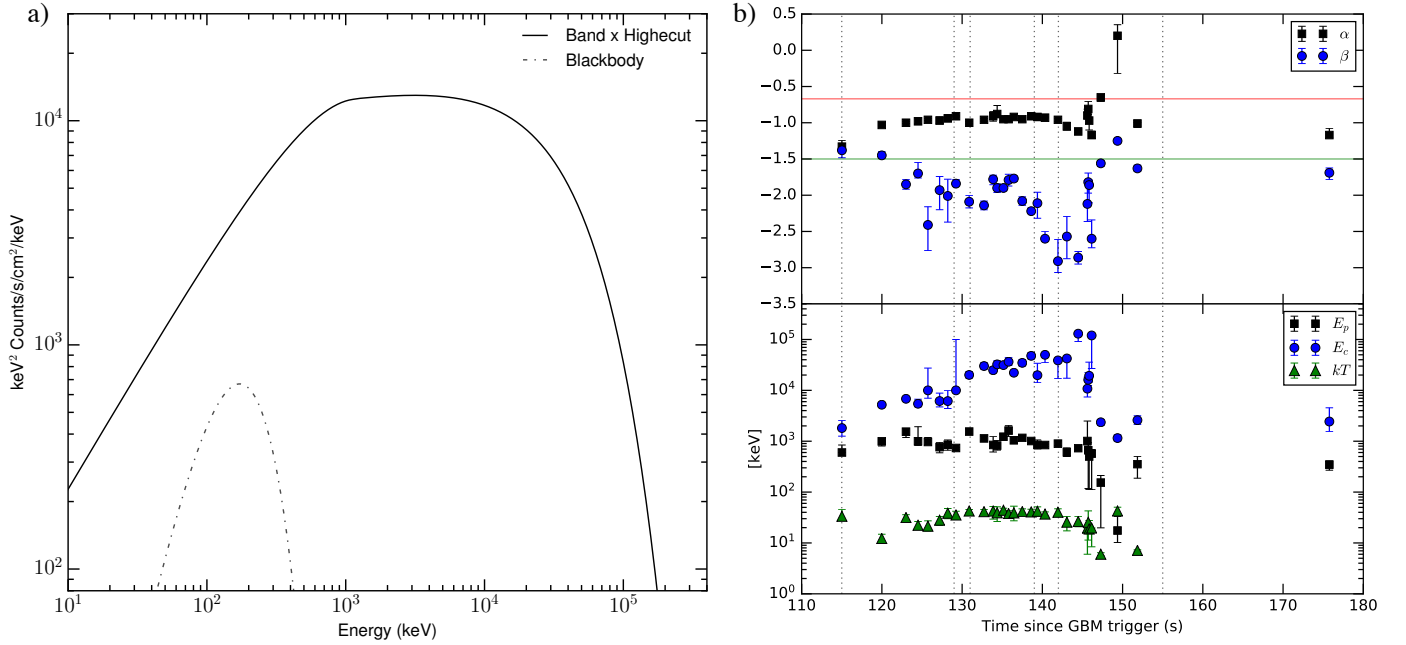


Figure 4. a) Figure shows the νF_ν plot of the best fit model, Band \times Hightecut (black solid line) + blackbody (black dash dot line), fitted to the brightest time interval, i.e 134.59 – 135.71 s. b) Upper panel shows the time evolution of α (black squares) and β (blue circles) of the Band function. The green and red horizontal lines in the upper panel mark the photon index of $\alpha = -1.5$ and $\alpha = -0.67$ corresponding to the fast and slow cooling synchrotron emissions respectively. In the lower panel, the time evolution of the Band E_p (black squares), the high energy cutoff E_c (blue circles) and the temperature of the blackbody component kT (green triangles) are shown. The three time intervals of polarization study are shown in black dotted vertical lines across the two panels.

Chand, V., Chattopadhyay, T., Oganessian, G., et al. 2019, *ApJ*, 874, 70
 Chand, V., Chattopadhyay, T., Iyyani, S., et al. 2018, *ApJ*, 862, 154
 Chattopadhyay, T., Vadawale, S. V., Rao, A. R., Sreekumar, S., & Bhattacharya, D. 2014, *Experimental Astronomy*, 37, 555
 Chattopadhyay, T., Vadawale, S. V., Aarthy, E., et al. 2017, *ArXiv e-prints*, arXiv:1707.06595
 Coburn, W., & Boggs, S. E. 2003, *Nature*, 423, 415
 Covino, S., & Gotz, D. 2016, *Astronomical and Astrophysical Transactions*, 29, 205
 Fishman, G. J. 2013, in *EAS Publications Series*, Vol. 61, *EAS Publications Series*, ed. A. J. Castro-Tirado, J. Gorosabel, & I. H. Park, 5–14
 Gehrels, N., & Swift. 2004, in *Bulletin of the American Astronomical Society*, Vol. 36, *American Astronomical Society Meeting Abstracts*, #116.01
 Ghisellini, G., & Lazzati, D. 1999, *MNRAS*, 309, L7
 Götz, D., Covino, S., Fernández-Soto, A., Laurent, P., & Bošnjak, Ž. 2013, *MNRAS*, 431, 3550
 Götz, D., Laurent, P., Antier, S., et al. 2014, *MNRAS*, 444, 2776

Götz, D., Laurent, P., Lebrun, F., Daigne, F., & Bošnjak, Ž. 2009, *ApJL*, 695, L208
 Granot, J. 2003, *ApJL*, 596, L17
 Guiriec, S., Connaughton, V., & et al. 2011, *ApJL*, 727, L33
 Iyyani, S. 2018, *Journal of Astrophysics and Astronomy*, 39, 75
 Iyyani, S., Ryde, F., Burgess, J. M., Pe’er, A., & Bégué, D. 2016, *MNRAS*, 456, 2157
 Iyyani, S., Ryde, F., & et al. 2013, *MNRAS*, 433, 2739
 Lazzati, D., & Begelman, M. C. 2009, *ApJL*, 700, L141
 Lazzati, D., Rossi, E., Ghisellini, G., & Rees, M. J. 2004, *MNRAS*, 347, L1
 Markwardt, C. B., Barthelmy, S. D., Cummings, J. R., et al. 2016, *GRB Coordinates Network, Circular Service*, No. 19840, #1 (2016), 19840
 McConnell, M. L. 2017, *New Astr. Rev.*, 76, 1
 McGlynn, S., Foley, S., McBreen, B., et al. 2009, *A&A*, 499, 465
 Meegan, C., Lichti, G., & et al. 2009, *ApJ*, 702, 791
 Mészáros, P. 2006, *Reports on Progress in Physics*, 69, 2259
 Pe’er, A. 2015, *Advances in Astronomy*, 2015, 907321
 Preece, R., Burgess, J. M., & et al. 2014, *Science*, 343, 51
 Racusin, J. L., Oates, S. R., & et al. 2011, *ApJ*, 738, 138

- Rao, A. R., Chand, V., Hingar, M. K., et al. 2016, *ApJ*, 833, 86
- Rutledge, R. E., & Fox, D. B. 2004, *MNRAS*, 350, 1288
- Singh, K. P., Tandon, S. N., Agrawal, P. C., et al. 2014, in *Society of Photo-Optical Instrumentation Engineers (SPIE) Conference Series*, Vol. 9144, Proc. SPIE, 91441S
- Stanbro, M., & Meegan, C. 2016, *GRB Coordinates Network*, Circular Service, No. 19835, #1 (2016), 19835
- Toma, K., Sakamoto, T., Zhang, B., et al. 2009, *ApJ*, 698, 1042
- Vadawale, S. V., Chattopadhyay, T., Rao, A. R., et al. 2015, *A&A*, 578, A73
- Vianello, G., Gill, R., Granot, J., et al. 2018, *ApJ*, 864, 163
- Wigger, C., Hajdas, W., Arzner, K., Güdel, M., & Zehnder, A. 2004, *ApJ*, 613, 1088
- Yonetoku, D., Murakami, T., Gunji, S., et al. 2011, *ApJL*, 743, L30
- . 2012, *ApJL*, 758, L1
- Zhang, S.-N., Kole, M., Bao, T.-W., et al. 2019, *Nature Astronomy*, 3, 258

ACKNOWLEDGMENTS

We would like to thank Dr Christoffer Lundman, Prof. Pawan Kumar and Dr Santosh Roy for enlightening discussions. This publication uses data from the *AstroSat* mission of the Indian Space Research Organisation (ISRO), archived at the Indian Space Science Data Centre (ISSDC). CZT-Imager is built by a consortium of institutes across India, including the Tata Institute of Fundamental Research (TIFR), Mumbai, the Vikram Sarabhai Space Centre, Thiruvananthapuram, ISRO Satellite Centre (ISAC), Bengaluru, Inter University Centre for Astronomy and Astrophysics, Pune, Physical Research Laboratory, Ahmedabad, Space Application Centre, Ahmedabad. This research has made use of *Fermi* data obtained through High Energy Astrophysics Science Archive Research Center Online Service, provided by the NASA/Goddard Space Flight Center. The Geant4 simulations for this paper were performed using the HPC resources at The Inter-University Centre for Astronomy and Astrophysics (IUCAA) and Physical Research Laboratory (PRL).

APPENDIX

A. SYSTEMATIC ERROR ESTIMATE IN POLARIZATION MEASUREMENT

Cadmium Zinc Telluride Imager (CZTI) on board AstroSat is an X-ray spectroscopic instrument and is experimentally verified for polarization measurement capability in 100-400 keV energy range for on axis sources (Vadawale et al. 2015). CZTI functions as a wide field monitor at energies > 100 keV because the CZTI collimators and other supporting structures become largely transparent above this energy. This enables it to detect GRBs and measure their polarization. In order to calculate the modulation factor for off-axis sources, a mass model of AstroSat was developed in Geant4 (version 4.10.02.p02). There are several possible sources of systematic errors in the measurement of polarization (Chattopadhyay et al. 2017). Below we list these sources and the error estimates are quoted for the case of GRB 160821A:

(i) An uncertainty can be induced in the observed μ due to different photon propagation paths through the spacecraft structures. This uncertainty is estimated by conducting $\sim 10^4$ Geant4 simulations of this burst with the same spectra and incident direction to produce the same number of observed Compton events. The uncertainty on μ is thus estimated to be $\sim 8 - 16\%$ according to the different number of Compton events. (ii) The selection of background is also expected to induce some systematic error. This was investigated by taking both pre and post GRB background independently as well as in combination, to determine the modulation amplitude. The uncertainty on μ due to this is found to be $< 1\%$. (iii) The effect of localization uncertainty is studied. GRB 160821A is localized at RA = 171.25 and Dec = +42.33 at ± 3 arcmin accuracy (Markwardt et al. 2016). The contribution of localization uncertainty on the obtained modulation amplitude and polarization angle is found to be $< 1\%$. (iv) The uncertainty associated with the spectral model of the GRB is investigated by varying the power law index within its estimated 1 sigma error and we find the associated uncertainty on the observed modulation amplitude to be $< 1\%$. (v) Another source of systematic error could be the unequal quantum efficiency of the CZTI pixels. The relative pixel efficiency across the CZTI plane is found to vary within $\leq 5\%$ which produces negligible false modulation amplitude.

In the μ_{100} estimations, the statistical error is quite small as the simulations are done for a large number (10^8) of incoming photons. The systematic errors are those associated with the sources (iii) and (iv) while the uncertainty associated with source (i) is estimated to be $\leq 1\%$. The value of μ_{100} strongly depends on the fitted polarization angle. The uncertainty associated with this in the estimation of PF is taken care of in the Monte Carlo process to obtain the posterior distribution of PF (described in Appendix B), where for each fitted polarization angle, the corresponding μ_{100} is used.

All these uncertainties are propagated into the reported values of the limits of the 68% confidence interval of two parameters of interest namely the observed polarization fraction and angle.

B. MONTE CARLO METHOD TO OBTAIN POSTERIOR DISTRIBUTIONS OF PF AND PA

The polarization signature in the GRB is estimated through the non-uniform azimuthal distribution of GRB counts. We calculate the normalized counts for 8 bins whose mid-values correspond to azimuthal angles: 0, 45, 90, 135, 180, 225, 270, 315 degrees. These angles are estimated in anti-clockwise direction when CZTI is viewed from top. The corrected modulation curves are fitted for large number of iterations (10 million) using Monte Carlo method for estimating the modulation factor and polarization angle, as follows:

- (a) For each azimuthal angle (η_i), and its corresponding normalized counts (y_i) and error ($y_{\text{err},i}$), we pick a random value ($y_{\text{ran},i}$), from a normal distribution which is defined by the mean value, $\mu_{\text{mean}} = y_i$ and the standard deviation, $\sigma_{\text{SD}} = y_{\text{err},i}$. A normal distribution is assumed because here, in the case of GRB 160821A, each azimuthal angular bin has over 20 Compton events (Cash 1979).
- (b) The A, B and ϕ_0 parameters of the fitting cosine function given in equation (1), are estimated for each set of randomly drawn $y_{\text{ran},i}$ (where $i = 1$ to 8) values via least square curve fitting method. For the fitted polarization angle, the corresponding interpolated value of μ_{100} from a table of μ_{100} values that were generated for a discrete grid of polarization angles via the Geant4 simulations of 100% polarized emission for the same GRB spectra and incoming direction, is chosen. Thereby, estimating the PF values.
- (c) The above two steps are repeated for a large number of times (10^7), thereby obtaining the various required likelihood distributions of PF and PA.
- (d) The obtained likelihood is then filtered through the prior condition such as the polarization fraction has to lie between 0 and 100 %. The simulation runs which satisfied the prior condition were used to generate the posterior distribution.
- (e) Finally, the respective 2D histogram of posterior distributions of PA and PF are made.

C. TIME RESOLVED SPECTROSCOPY

For analysis of the *Fermi* GBM data, three sodium iodide (NaI) detectors with the highest count rates were chosen, namely n6, n7 and n9. These detectors observed the GRB at an off-axis angle less than 40° . In addition, the Bismuth gallium oxide (BGO) detector BGO 1, which had the strongest detection, was chosen for analysis. LAT data (> 100 MeV) belonging to the P8_TRANSIENT020E class and its corresponding instrument response were used, whereas, the LAT-LLE spectra (30 - 130 MeV) were obtained using the same method as that for GBM data. The spectrum for each *Fermi* detector was extracted using the software *Fermi* Burst Analysis GUI v 02-01-00p1 (gtburst3⁶). The background was obtained by fitting a polynomial function to the data regions before and after the GRB for time intervals, $T_0 - 410$ s to $T_0 - 10$ s and $T_0 + 210$ s to $T_0 + 250$ s, respectively.

A joint spectral analysis of *Fermi* GBM along with LAT-LLE and LAT data was carried out in Xspec (Arnaud 1996) 12.9.0n software and Pg-stat (Arnaud 2013) statistic was used. For NaI data, energies between 30 keV – 40 keV corresponding to iodine K-edge and extreme edges such as energies below 10 keV and above 850 keV were removed. In case of BGO, LAT LLE and LAT, data between energies 300 keV – 10 MeV, 30 MeV – 130 MeV and 100 MeV – 5 GeV were used respectively.

For time resolved spectroscopy of the burst, time intervals were defined using Bayesian Blocks (BB) algorithm on the detector (n6) with largest number of counts. In the tails of the emission episode, due to low signal to noise ratio, certain blocks were combined to get a larger time interval so that good spectral constraints could be obtained.

For estimating the effective area correction⁷ for NaI and LAT detectors, the bright time bins were simultaneously fitted with the best fit model i.e blackbody + Band \times Hightecut multiplied with a constant of normalization, while the constant of normalization of the BGO 1 detector was fixed to unity. The relative normalization constants $0.97_{-0.01}^{+0.01}$ for n6, $0.92_{-0.01}^{+0.01}$ for n7, $0.94_{-0.01}^{+0.01}$ for n9 and $0.84_{-0.06}^{+0.06}$ for LAT were obtained. Throughout the time resolved spectral analysis, the effective area corrections for the detectors were frozen to these obtained values.

C.1. Statistical Significance test

We conduct Monte Carlo simulations in order to ascertain the statistical significance of the deviations in the spectrum from a pure Band function, which have been modelled using a blackbody and a cutoff at lower and higher energies respectively (see the fit residuals in Figure 5). Since this process is computationally intensive here we present the simulation study done for the brightest time bin (134.59 - 135.71 s) only, and adopt the obtained Δ Pg-stat distribution as a reference to assess the statistical significance of these components in other time bins.

a) Blackbody

The difference in statistic i.e Δ Pg-stat, obtained for the model BB + Band \times Hightecut (f_{BHec}) from f_{BHec} is 24.5. We assume the model f_{BHec} with the best fit model parameters as the null hypothesis (H0) and generate nearly 40,000 realizations and its corresponding background spectra using the *fakeit* command in Xspec. Each of these realizations

⁶ <https://fermi.gsfc.nasa.gov/ssc/data/analysis/scitools/gtburst.html>

⁷ An effective area of an instrument translates to its sensitivity, which can be different at different energies and off axis angles from the axis of the instrument. Here in order to do a combined spectral analysis of the data from different instruments like NaI, BGO and LAT, a correction needs to be applied between these instruments keeping one of them as the reference. This is estimated by multiplying a constant, independent of energy, to the normalization of the spectral model chosen for each instrument during the spectral analysis.

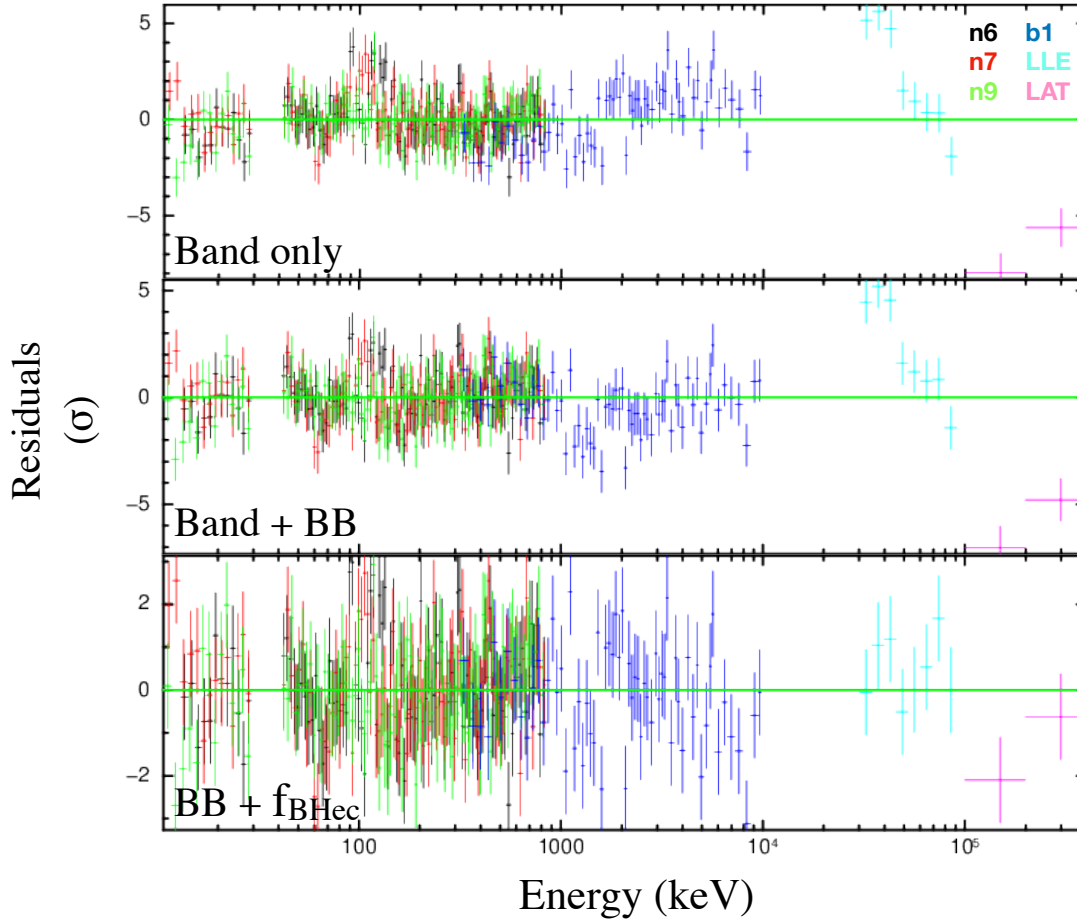


Figure 5. The residuals obtained for the different models, Band, Band + BB and $BB + f_{BHec}$, fits done to the spectral data of the brightest time interval are shown.

are then fit with the null hypothesis model f_{BHec} and the alternate hypothesis (H1) model $BB + f_{BHec}$, and the respective Δ Pg-stat values are recorded. The probability to observe any Δ Pg-stat of > 24.5 is found to be $10^{-4.3}$ (Figure 6a) which corresponds to a significance level of $\sim 4\sigma$.

b) Hightecut

The Δ Pg-stat, obtained for the model $BB + f_{BHec}$ from $BB + \text{Band}$ is 201. In this case, we assume the model $BB + \text{Band}$ with the best fit model parameters as the H0 and generate nearly 54,000 realizations and its corresponding background spectra. The model $BB + f_{BHec}$ is the H1 and the respective complementary cumulative distribution of Δ Pg-stat is obtained. The probability to obtain Δ Pg-stat = 14 is $10^{-4.5}$ (Figure 6b) which indicates that the probability to obtain any Δ Pg-stat > 201 is $\ll 10^{-4.5}$ which corresponds to a significance level of $> 4.2\sigma$. Thus, the addition of hightecut to the Band function is highly significant.

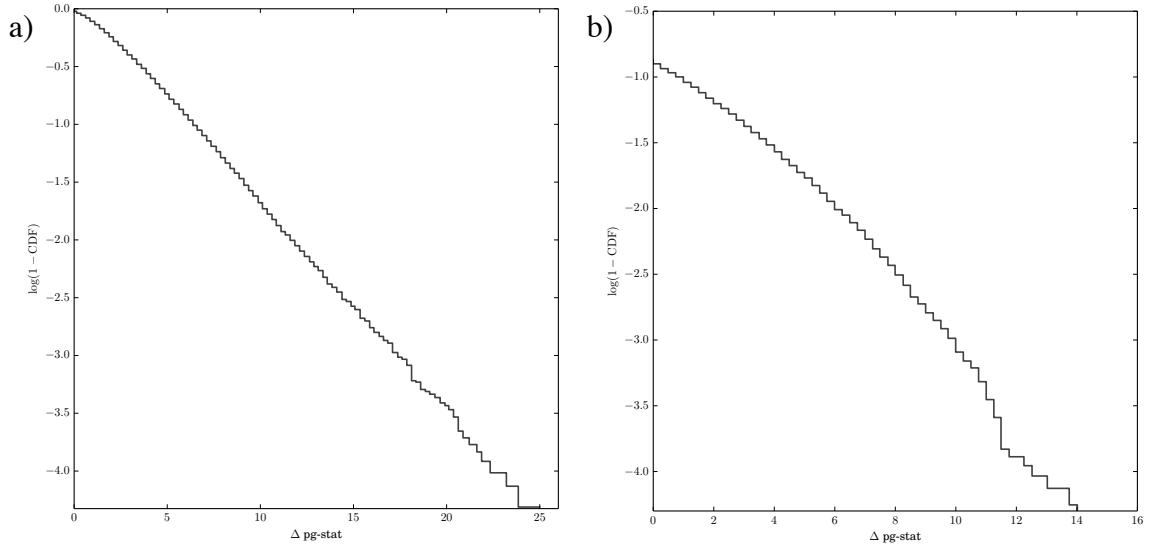


Figure 6. The complementary cumulative distribution function (CDF) of the pg-stat obtained for models a) f_{BHec} function vs blackbody + f_{BHec} , and b) blackbody + Band function vs blackbody + f_{BHec} are shown.